

RHIC Critical Point Search: Assessing STAR's Capabilities

Paul Sorensen for the STAR Collaboration

Brookhaven National Laboratory

E-mail: prsorensen@bnl.gov

In this report we discuss the capabilities and limitations of the STAR detector to search for signatures of the QCD critical point in a low energy scan at RHIC. We find that a RHIC low energy scan will cover a broad region of interest in the nuclear matter phase diagram and that the STAR detector — a detector designed to measure the quantities that will be of interest in this search — will provide new observables and improve on previous measurements in this energy range.

*The 3rd edition of the International Workshop — The Critical Point and Onset of Deconfinement —
July 3-7 2006
Galileo Galilei Institute, Florence, Italy*

Experiments at RHIC have found evidence that a strongly coupled quark-gluon plasma is created in heavy-ion collisions at $\sqrt{s_{NN}} = 200$ GeV [1]. At these high energies the baryon chemical-potential (μ_B) extracted from thermal model fits is small (approximately 0.025 GeV) [2]. Lattice calculations indicate that for $\mu_B = 0$, as the temperature (T) of nuclear matter is increased the transition from confined to deconfined matter is a smooth crossover [3] and that the chiral and deconfinement transitions happen at approximately the same temperature [4, 5]. Model calculations, however, suggest that for $T = 0$, the transition as μ_B is increased is first order [6]. If this is the case, then a critical point should exist where the transition changes from first order, to a smooth-crossover [7].

It may be possible to ascertain the (T, μ_B) coordinates of the critical point by decreasing the collision energy for heavy-ion collisions at RHIC [8]: μ_B increases with decreasing $\sqrt{s_{NN}}$. A non-monotonic dependence of variables on $\sqrt{s_{NN}}$ and an increase in event-by-event fluctuations should become apparent near the critical point [9, 10]. The energy scan at the CERN-SPS ($6.3 < \sqrt{s_{NN}} < 17.3$ GeV) found some possible signatures of a critical point, but the evidence remains inconclusive and sometimes contradictory [11, 12, 13]. Using a collider to perform such an energy scan, instead of fixed-targets, should provide two important advantages: acceptance won't change with $\sqrt{s_{NN}}$ and track-density at mid-rapidity will only vary slowly [14]. In addition, the detectors at RHIC are of a more advanced design [15]. Figure 1 shows lattice QCD estimates of the critical temperature T_C for $\mu_B = 0$ [16], lattice QCD estimates of the location of the critical point [17] and an estimate of the region that can be covered by a RHIC low energy scan. We find that the RHIC low energy scan will cover a broad region of interest in the T, μ_B plane [18].

In this report, we will assess the capabilities of the STAR detector [19] at RHIC to perform a critical point search in which the center-of-mass energy of collisions may be reduced to as low as $\sqrt{s_{NN}} \sim 4.5$ GeV. We focus on several key measurements: yields, fluctuations in particle ratios, and elliptic flow. The STAR detector was designed for these measurements so we expect it to perform well. We present simulations that indicate this is the case. We also indicate where potential difficulties may arise.

1. STAR Detector

The layout of the STAR detector system as it was for Run-2 is shown in Figure 2. The active subsystems included two RHIC-standard zero-degree calorimeters (ZDCs) that detect spectator neutrons, a central trigger barrel (CTB) that measures event multiplicity, a time-of-flight detector, an electromagnetic calorimeter to measure photons, electrons and the transverse energy of events, and four tracking detectors. The tracking detectors are the main TPC, two forward TPCs, and the silicon vertex tracker (SVT).

The TPC is STAR's primary detector [20] and can track up to $\sim 4 \times 10^3$ particles per event. For collisions in its center, the TPC covers the pseudo-rapidity region $|\eta| < 1.8$. It can measure particle p_T within the approximate range $0.07 < p_T < 30$ GeV/c. The momentum resolution $\delta p/p$ depends on η and p_T but for most tracks $\delta p/p \sim 0.02$. The full azimuthal coverage of the STAR detector ($-\pi < \phi < \pi$) makes it ideal for detecting weak decay vertices, reconstructing resonances, measuring v_2 and event-by-event fluctuations.

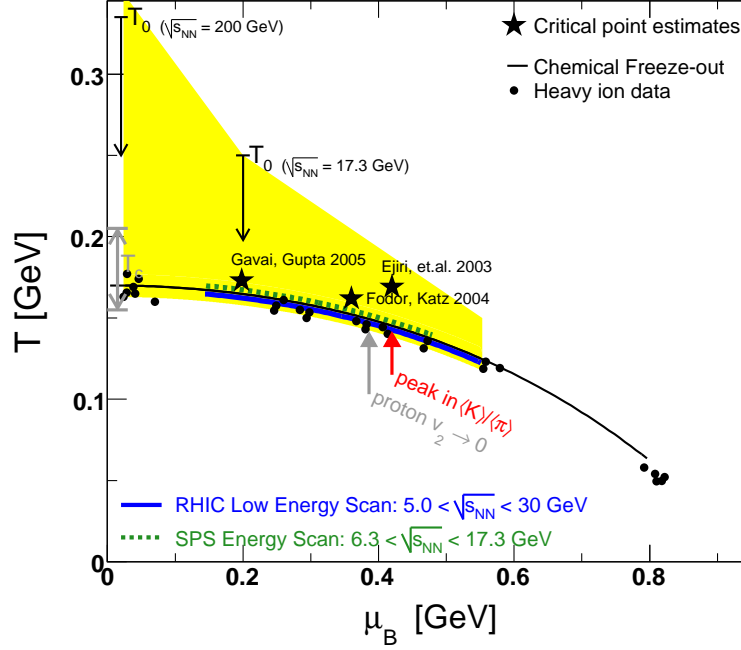


Figure 1: A sketch of the phase diagram of nuclear matter showing the chemical freeze-out curve, points from fits to heavy-ion collision data, estimates of the initial temperatures achieved in heavy-ion collisions, lattice QCD estimates of the critical temperature T_C for $\mu_B = 0$ [16], and lattice QCD estimates of the location of the critical point [17]. The shaded region shows an estimate of the region of the phase diagram that can be covered by a low energy scan at RHIC.

The read-out rate for the STAR TPC is ~ 100 Hz. For $\sqrt{s_{NN}} < 20$ GeV, without electron cooling upgrades to RHIC, the bunch crossing and event rates will be much slower than the TPC read-out rate. As such, STAR will be able to record every detected event. To trigger on the occurrence of a collision, STAR will need to use its Beam-Beam Counters (BBC). In Figure 3 (right) UrQMD [21] simulations of the multiplicity of tracks versus pseudo-rapidity are shown. Although the Zero-degree Calorimeters will not register a signal for collisions with $\sqrt{s_{NN}} < 20$ GeV, tracks will impinge on STARs BBCs. Table 1 lists the number of charged particles within the BBC acceptance for several energies and centralities. In all cases, the number of tracks is sufficient to detect the occurrence of a collision.

Table 1: Number of particles impinging on STARs Beam-Beam Counters for Au+Au collisions in UrQMD [21] simulations.

impact parameter (fm)	$\sqrt{s_{NN}} = 5$ GeV		$\sqrt{s_{NN}} = 8.75$ GeV	
	BBC Inner	BBC Outer	BBC Inner	BBC Outer
$0 < b < 3$	5	27	12	54
$3 < b < 6$	11	30	21	57
$6 < b < 9$	22	35	39	40

STARs ability to effectively trigger on events at these low energies coupled with our proven ability to statistically extract particle identification information over a broad p_T [22] range will

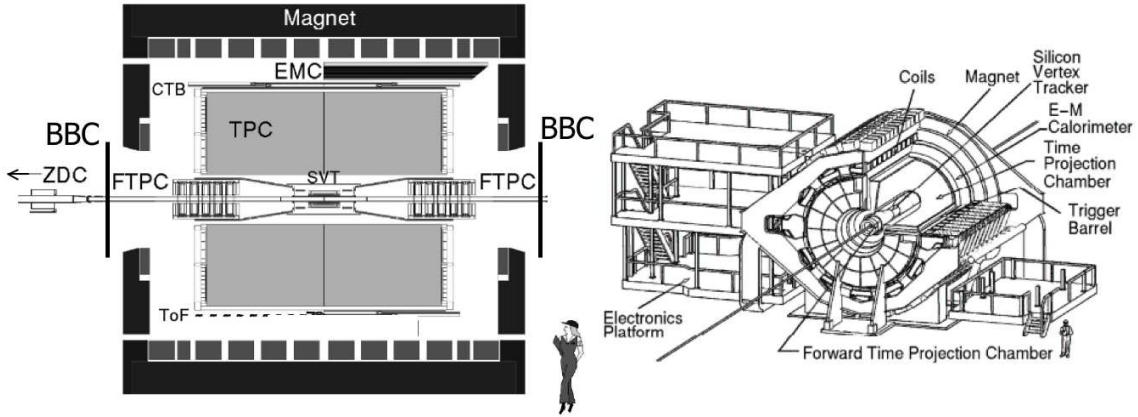


Figure 2: The STAR detector [19]: a cross-section view (left panel) and perspective view (right panel). STAR is an azimuthally symmetric, large acceptance, solenoidal detector designed to measure many observables simultaneously. The detector consists of several subsystems and a large Time Projection Chamber (TPC) [20] located in a 0.5 Tesla solenoidal analyzing magnet.

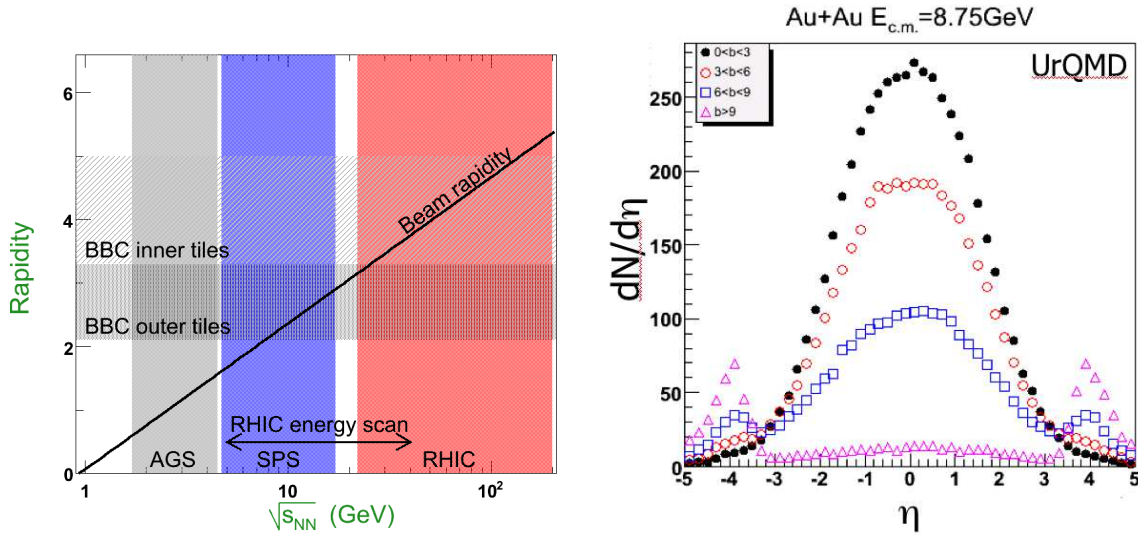


Figure 3: Beam rapidity versus $\sqrt{s_{NN}}$ (left panel) and the corresponding acceptance for STARs Beam-beam counters. UrQMD simulation of charged hadron yields for $\sqrt{s_{NN}} = 8.75$ GeV (right panel).

make measurements of particle spectra and ratios possible. As such, T and μ_B can be extracted from statistical model fits. We note, however, that many of these particle identification methods are statistical and therefore cannot be used to identify particles on an event-by-event basis: as will be needed for particle ratio fluctuation measurements. For event-by-event particle identification over a broad p_T range, a Time-of-Flight detector [23] is being constructed that will cover 2π in azimuth and $-1 < \eta < 1$ in pseudo-rapidity. This detector upgrade is expected to be finished by 2010.

2. Analysis

The STAR detector will be able to improve on many of the measurements of interest in a

critical point search. Since event rates are not expected to be particularly large (approximately 5 Hz at $\sqrt{s_{NN}} = 5$ GeV), rare probes such as the J/ψ will likely be inaccessible. Below, we discuss some of the key measurements for a low energy scan at RHIC. In these proceedings we do not discuss in detail such important measurements as HBT [24], v_1 [25], balance functions [26] and multiplicity, net charge, or $\langle p_T \rangle$ fluctuations [27]: all of which are measurements STAR will be able to perform well. Rather, we present a subset of measurements — v_2 , v_2 fluctuations, and dynamical fluctuations of the kaon-to-pion ratio — in order to illustrate the STAR detectors capabilities for a critical point search at RHIC.

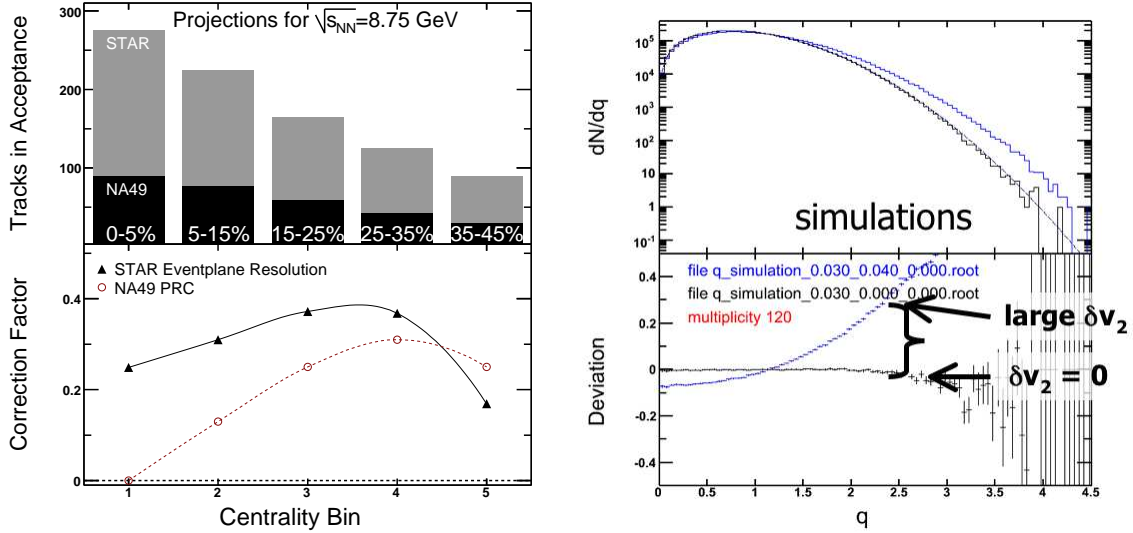


Figure 4: Top left: The expected number of tracks within the STAR TPC acceptance and simulations of the event-plane resolution correction factor (bottom left). The left figure also shows the corresponding NA49 quantities for comparison [12]. Top right: The expected shape of the distribution of the length of the q -vector (curve) for the given values of v_2 and simulation results (histograms) with and without v_2 fluctuations. Bottom right: Deviations between simulations and the expected shape due to v_2 fluctuations demonstrating that the distribution of the length of the q -vector distribution is sensitive to v_2 fluctuations.

A key indicator of the ability to measure elliptic flow is the reaction-plane resolution correction factor [28]. When the factor is large (close to unity), the direction of the reaction plane can be well determined on an event-by-event basis and fewer events will be needed for an accurate determination of v_2 . The resolution depends on the number of tracks used and the magnitude of the event asymmetry. For the most peripheral events the small number of tracks available reduces the resolution while for the most central events the symmetry of the collision overlap region degrades it. For Au+Au collisions, the resolution is typically greatest at a centrality corresponding to roughly 20–30% of the collision cross-section [29]. In Fig. 4 (bottom left) we show the expected resolution correction factor for Au+Au collisions at $\sqrt{s_{NN}} = 8.75$ GeV in the STAR detector along with the resolution correction factor achieved by the NA49 collaboration. The observed v_2 value must be divided by the resolution correction factor to get the true v_2 . When this factor is closer to zero than one, both the observed v_2 and the statistical errors must be scaled up by a large number. A large improvement is expected with the STAR detector due to its full azimuthal coverage extending over 2 units of pseudo-rapidity. This leads to a large increase in the number tracks available for the mea-

surement of v_2 . Figure 4 (top left) shows the number of tracks available for analysis by NA49 and STAR.

In the most peripheral collisions the resolution correction factor for NA49 is apparently larger than our simulation results for STAR. Given the larger coverage of the STAR detector, it is unlikely that the NA49 detector can have a better resolution. Either the STAR resolution is under-estimated for this bin or the NA49 measurements lose accuracy where the multiplicity is at its lowest value.

The right panel of Fig. 4 shows the distribution of the length of the flow vector q from simulations [30]. The histograms in the top panel are the simulated data with and without v_2 fluctuations. The curve shows the expected shape of the distribution derived from the central limit theorem [31]. The difference between the two histograms shows how much the distribution changes if v_2 fluctuates from event-to-event. The bottom panel shows deviations between the simulated data and the expected shape. The simulations use $v_2 = 0.03$, and a multiplicity of 120 tracks. v_2 fluctuations in the simulation are Gaussian with either zero width or a width of 0.04. The figure demonstrates that v_2 fluctuations can be measured using the distribution of the length of the flow vector. This measurement will remove a dominant source of systematic uncertainty in v_2 measurements and provide a robust critical point signature. Preliminary results have already been presented [30, 32].

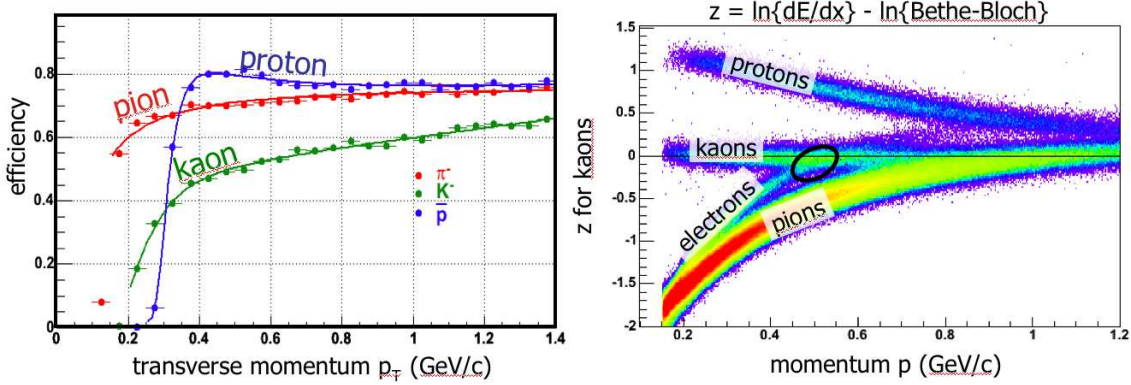


Figure 5: Left panel: The efficiency versus p_T for detecting pions, kaons, and protons with the STAR detector. Right panel: The z -variable for kaons derived from ionization energy loss measurements dE/dx in the STAR TPC. This variable illustrates how well a particular particle species can be distinguished from other particles.

The left panel of Fig. 5 shows the STAR detectors efficiency for detecting pions, kaons, and protons versus p_T . The efficiency for detecting kaons is lower than for pions or protons. This reduction is due to the failure to detect kaons that decay before they traverse the TPC volume. In a fixed target experiment, the momentum boost in the lab frame makes it much less likely that a weak-decay will occur before the kaon has traversed the detector. The efficiency near the kaon $\langle p_T \rangle$ is approximately 45%.

The right panel of Fig. 5 shows the z -variable for kaons which illustrates the ability of STAR to distinguish between kaons and other particle species using ionization energy loss measurements dE/dx in the TPC volume. z is the logarithm of the ratio of the measured dE/dx to the expected dE/dx [33] for a particular particle species. Kaons can be identified with good certainty when the particle momentum is below 400 MeV. Above that value though, electrons begin to contaminate the

kaon sample. Many electrons come from pion decays so they need to be excluded from the kaon sample in order to accurately extract the kaon-to-pion ratio event-by-event. In addition, since pions can yield more than one electron in their decay chain, mixed events may not be able to account for electron contamination of the kaon sample. Requiring a good purity for the kaon sample will further reduce the efficiency for kaon detection: typical kaon efficiency values in STAR kaon-to-pion fluctuation analyses can be as low as 10%–15% [34]. For this reason, these measurements are challenging.

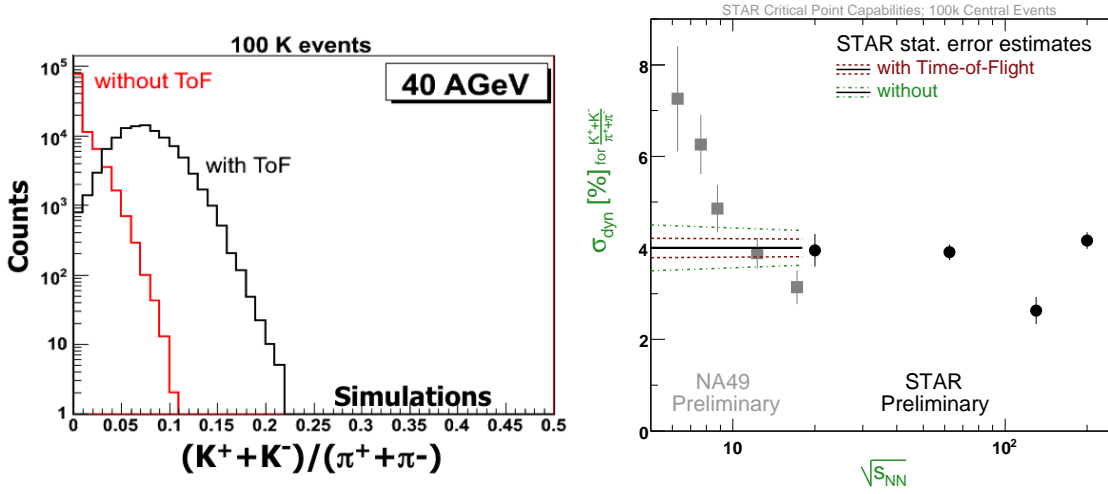


Figure 6: Left panel: Simulation of the event-by-event kaon-to-pion ratio for Au+Au collisions at $\sqrt{s_{NN}} = 8.76$ GeV with or without a Time-of-Flight (TOF) detector available to improve particle identification. Right panel: Dynamic fluctuations of the kaon-to-pion ratio measured by STAR [34] and NA49 [13] along with estimates of the errors for 100,000 central Au+Au collisions with, or without TOF information.

In Fig. 6 (left) we show simulation results for the event-by-event distribution of the kaon-to-pion ratio observed by the STAR detector with or without the TOF upgrade. The simulations are for 100,000 central Au+Au collisions at $\sqrt{s_{NN}} = 8.76$ GeV. The reduction of the size of the kaon sample without the TOF upgrade causes the distribution to narrow and squeeze against the zero axis: in many events, no kaons are found. This may make it more difficult to extract a meaningful width relative to mixed events for the distribution.

In the right panel of Fig. 6 we show preliminary STAR [34] and NA49 [13] measurements of the width of the dynamic kaon-to-pion fluctuations: these are extracted from the difference between the width of real and mixed events. We also show estimates of the statistical errors expected with the STAR detector for 100,000 central Au+Au collisions at $\sqrt{s_{NN}} < 18$ GeV. The TOF detector allows the errors to be reduced by a factor of two compared to STAR without the TOF. The errors are similar to or smaller than the corresponding NA49 errors. We note however that systematic errors on this measurement are dominant. In particular, we find that misidentifying 0.5% of pions as kaons in our simulations reduces the width of the distribution by 5%. That systematic uncertainty is as large as the expected signal. The TOF upgrade is therefore important for this measurement since it will significantly improve the purity of the kaon sample.

3. Conclusions

We've investigated the performance capabilities of the STAR detector for a low energy scan at RHIC. We find that STAR will be able to effectively trigger on collisions at these low energies and given the same number of events will be able to significantly improve on previous measurements. Measurements taken in a collider geometry will have smaller $\sqrt{s_{NN}}$ -point-to-point systematic errors than for a fixed target geometry. The efficiency for detecting kaons however will be smaller due to weak-decays of the kaon. If TOF information is not available the available sample of kaons will become even smaller and dynamical kaon-to-pion fluctuation measurements will become challenging. Elliptic flow measurements will be significantly improved because of the STAR detectors large acceptance at mid-rapidity and symmetric two- π azimuthal coverage. Elliptic flow fluctuation measurements based on the shape of the flow vector distribution will also be possible. Although not shown here, other measurements such as v_1 , HBT, and $\langle p_T \rangle$ fluctuations will be made much better by the STAR detector than by previous experiments which had smaller acceptances which changed with $\sqrt{s_{NN}}$.

In summary, a RHIC low energy scan to search for the QCD critical point will cover a broad region of interest in the nuclear matter phase diagram. The STAR detector — a detector designed to measure the quantities that will be of interest in this search — will provide new observables and will improve on previous measurements in this energy range.

References

- [1] I. Arsene *et al.* [BRAHMS Collaboration], Nucl. Phys. A **757**, 1 (2005); B. B. Back *et al.* [PHOBOS Collaboration], Nucl. Phys. A **757**, 28 (2005); J. Adams *et al.* [STAR Collaboration], Nucl. Phys. A **757**, 102 (2005); K. Adcox *et al.* [PHENIX Collaboration], Nucl. Phys. A **757**, 184 (2005).
- [2] J. Cleymans, H. Oeschler, K. Redlich and S. Wheaton, Phys. Rev. C **73**, 034905 (2006).
- [3] F. R. Brown *et al.*, Phys. Rev. Lett. **65**, 2491 (1990).
- [4] A. Mocsy, F. Sannino and K. Tuominen, Phys. Rev. Lett. **92**, 182302 (2004).
- [5] F. Karsch and M. Lutgemeier, Nucl. Phys. B **550**, 449 (1999).
- [6] M. Asakawa and K. Yazaki, Nucl. Phys. A **504**, 668 (1989); A. Barducci, R. Casalbuoni, S. De Curtis, R. Gatto and G. Pettini, Phys. Lett. B **231**, 463 (1989); A. Barducci, R. Casalbuoni, S. De Curtis, R. Gatto and G. Pettini, Phys. Rev. D **41**, 1610 (1990); A. Barducci, R. Casalbuoni, G. Pettini and R. Gatto, Phys. Rev. D **49**, 426 (1994); J. Berges and K. Rajagopal, Nucl. Phys. B **538**, 215 (1999); M. A. Halasz, A. D. Jackson, R. E. Shrock, M. A. Stephanov and J. J. M. Verbaarschot, Phys. Rev. D **58**, 096007 (1998); O. Scavenius, A. Mocsy, I. N. Mishustin and D. H. Rischke, Phys. Rev. C **64**, 045202 (2001); N. G. Antoniou and A. S. Kapoyannis, Phys. Lett. B **563**, 165 (2003); Y. Hatta and T. Ikeda, Phys. Rev. D **67**, 014028 (2003).
- [7] M. A. Stephanov, Prog. Theor. Phys. Suppl. **153**, 139 (2004) [Int. J. Mod. Phys. A **20**, 4387 (2005)].
- [8] Many details regarding a possible low energy scan at RHIC can be found in talks presented at the RIKEN BNL Research Center Workshop, "Can We Discover the QCD Critical Point at RHIC" which can be found at the following web-site: <https://www.bnl.gov/riken/QCDRhic/talks.asp>.
- [9] M. A. Stephanov, K. Rajagopal and E. V. Shuryak, Phys. Rev. Lett. **81**, 4816 (1998) [arXiv:hep-ph/9806219].

- [10] S. Ejiri, F. Karsch and K. Redlich, Phys. Lett. B **633**, 275 (2006).
- [11] S. V. Afanasiev *et al.* [The NA49 Collaboration], Phys. Rev. C **66**, 054902 (2002).
- [12] C. Alt *et al.* [NA49 Collaboration], Phys. Rev. C **68**, 034903 (2003).
- [13] C. Roland *et al.* [NA49 Collaboration], J. Phys. G **30**, S1381 (2004).
- [14] G. Roland "Experimental Overview and Prospects for RHIC," RIKEN BNL Research Center Workshop: Can We Discover the QCD Critical Point at RHIC?, <https://www.bnl.gov/riken/QCDRhic/talks.asp>.
- [15] T. Ludlam, Nucl. Instrum. Meth. A **499**, 428 (2003).
- [16] C. Bernard *et al.* [MILC Collaboration], Phys. Rev. D **71**, 034504 (2005); M. Cheng *et al.*, Phys. Rev. D **74**, 054507 (2006); Y. Aoki, Z. Fodor, S. D. Katz and K. K. Szabo, Phys. Lett. B **643**, 46 (2006).
- [17] F. Karsch, C. R. Allton, S. Ejiri, S. J. Hands, O. Kaczmarek, E. Laermann and C. Schmidt, Nucl. Phys. Proc. Suppl. **129**, 614 (2004); Z. Fodor and S. D. Katz, JHEP **0404**, 050 (2004); R. V. Gavai and S. Gupta, Phys. Rev. D **71**, 114014 (2005).
- [18] The upper reach of this region is based on estimates of the initial temperature achieved in heavy-ion collisions. See e.g.: D. Y. Peressounko and Yu. E. Pokrovsky, photons," arXiv:hep-ph/0009025; U. W. Heinz, arXiv:nucl-th/0512051.
- [19] K. H. Ackermann *et al.* [STAR Collaboration], Nucl. Instrum. Meth. A **499**, 624 (2003).
- [20] M. Anderson *et al.*, Nucl. Instrum. Meth. A **499**, 659 (2003).
- [21] M. Bleicher *et al.*, J. Phys. G **25**, 1859 (1999).
- [22] M. Shao, O. Y. Barannikova, X. Dong, Y. Fisyak, L. Ruan, P. Sorensen and Z. Xu, Nucl. Instrum. Meth. A **558**, 419 (2006).
- [23] F. Geurts *et al.*, Nucl. Instrum. Meth. A **533**, 60 (2004); W. J. Llope, Nucl. Instrum. Meth. B **241**, 306 (2005).
- [24] C. Adler *et al.* [STAR Collaboration], Phys. Rev. Lett. **87**, 082301 (2001).
- [25] J. Adams *et al.* [STAR Collaboration], Phys. Rev. Lett. **92**, 062301 (2004).
- [26] J. Adams *et al.* [STAR Collaboration], Phys. Rev. Lett. **90**, 172301 (2003).
- [27] J. Adams *et al.* [STAR Collaboration], Phys. Rev. C **68**, 044905 (2003); J. Adams *et al.* [STAR Collaboration], Phys. Rev. C **71**, 064906 (2005); J. Adams *et al.* [STAR Collaboration], Phys. Rev. C **72**, 044902 (2005); J. Adams *et al.* [STAR Collaboration], J. Phys. G **32**, L37 (2006).
- [28] A. M. Poskanzer and S. A. Voloshin, Phys. Rev. C **58**, 1671 (1998).
- [29] K. H. Ackermann *et al.* [STAR Collaboration], Phys. Rev. Lett. **86**, 402 (2001); C. Adler *et al.* [STAR Collaboration], Phys. Rev. Lett. **87**, 182301 (2001); C. Adler *et al.* [STAR Collaboration], Phys. Rev. Lett. **89**, 132301 (2002); C. Adler *et al.* [STAR Collaboration], Phys. Rev. C **66**, 034904 (2002).
- [30] P. Sorensen, arXiv:nucl-ex/0612021.
- [31] J. Y. Ollitrault, arXiv:nucl-ex/9711003; N. Borghini, P. M. Dinh and J. Y. Ollitrault, Phys. Rev. C **63**, 054906 (2001).
- [32] B. Alver *et al.* [PHOBOS Collaboration], arXiv:nucl-ex/0608025.
- [33] H. Bichsel, Nucl. Instrum. Meth. A **562**, 154 (2006).
- [34] S. Das [STAR Collaboration], arXiv:nucl-ex/0610044; T. K. Nayak, J. Phys. G **32**, S187 (2006).